Time-Harmonic Finite Element Machine Analysis Including Higher Harmonic Air Gap Fields

H. De Gersem[1], K. Hameyer[2], and T. Weiland[1]

[1]Technische Universität Darmstadt, Computational Electromagnetics Laboratory (TEMF)
Schloßgartenstraße 8, D-64404 Darmstadt, Germany.
phone: +49 6151 162361 – fax: +49 6151 164611 – e-mail: DeGersem/Weiland@temf.tu-darmstadt.de

[2]Katholieke Universiteit Leuven, Dept. ESAT, Div. ELECTA
Kasteelpark Arenberg 10, B-3001 Leuven-Heverlee, Belgium
phone: +32 16 321020 – fax: +32 16 321985 – e-mail: Kay.Hameyer@esat.kuleuven.ac.be

***Abstract* – Motional eddy current effects due to higher harmonic air gap fields in electrical machines are incorporated in time-harmonic finite element machine models by a spectral decomposition of the air gap field and the distribution of higher harmonic components to additional rotor models. The method is illustrated for a shaded-pole motor and a capacitor motor.**

1. Introduction

Virtual prototyping of electrical machines requires the simulation of stationary operating conditions, e.g. speed-torque characteristics. For three-phase (3ph) induction machines (IMs), 2D time-harmonic finite element (FE) analysis attains a sufficient accuracy for many technical models [1]. The key point is that the relevant phenomena in both stator and rotor vary in time at a single frequency, excitation and slip frequency respectively, and hence can be resolved by a time-harmonic simulation scheme [2, 3]. Time-harmonic simulation is no longer an option if components with different harmonic orders become important, e.g. in 3ph IMs with fault conditions or in single-phase IMs. Turning to transient simulation is expensive and therefore not always recommended. A time-harmonic simulation scheme accounting for both the forward and backward rotating air gap field in single-phase induction machines is described in [4]. In this paper, the time-harmonic FE approach is generalised to situations with an arbitrary set of relevant air gap field harmonics. The new approach is generally applicable and is substantially less expensive for simulating steady-state machine operation compared to the transient approach.

2. Finite element machine models

Two common approaches for simulating electrical machines are the transient approach and the time-harmonic approach. The transient approach consists of solving the partial differential equation (PDE)

$$\nabla \times (\nu \nabla \times \mathbf{A}) + \sigma \frac{\partial \mathbf{A}}{\partial t} = -\sigma \nabla V \tag{1}$$

with $\mathbf{A}$ the magnetic vector potential, ν the reluctivity, σ the conductivity and V the voltage, by time stepping [5, 6]. The transient approach accounts for motional eddy currents by the Lagrange technique: between two successive time steps, the previous solution is azimuthally moved together with the rotor part. Accordingly, the interface conditions between stator and rotor are updated. The relative motion of both motor parts can be modelled by a moving band technique [7], a hybrid FE, boundary-element approach [8], discontinuous finite elements [9] or a sliding surface technique [10]. In the last case, it is advantageous to allow for non-matching discretisations at the interface, possibly resolved by mortar finite elements [11]. Transient methods are however too expensive when only stationary operations have to be simulated.

For electrical machines excited by alternating current sources and rotating at constant velocities, formulations in frequency domain are preferred. The simplest case is when only one frequency f is present in the excitating voltages. Then, one can adopt the time-harmonic formulation

$$\nabla \times (\nu \nabla \times \underline{\mathbf{A}}) + \mathrm{j}\omega\sigma \underline{\mathbf{A}} = -\sigma \nabla \underline{V} \tag{2}$$

with the phasor $\underline{\mathbf{A}}$ related to the magnetic vector potential $\mathbf{A}$ by

$$\mathbf{A}(x,y,z,t) = \mathrm{Re}\left\{\underline{\mathbf{A}}(x,y,z)e^{\mathrm{j}\omega t}\right\} \ , \tag{3}$$

ν the reluctivity, σ the conductivity, $\underline{V}$ the phasor of the voltage and $\omega = 2\pi f$ the pulsation.

For many cylindrical machines, a 2D FE model of the cross-section of the machine, extended with an equivalent circuit modelling the electric connections at the front and rear machine ends, achieves a sufficient accuracy [12]. Then, the vectorial PDE (2) simplifies to a scalar PDE in terms of the z-component $\underline{A}_z$ of $\underline{\mathbf{A}}$:

$$-\nabla_{xy} \cdot (\nu \nabla_{xy} \underline{A}_z) + \mathrm{j}\omega\sigma \underline{A}_z = \frac{\sigma}{\ell_z} \Delta \underline{V} \tag{4}$$

with ℓ_z the device length and $\Delta\underline{V}$ the voltage drop between the machine's front and back side. The discretisation of (4) by linear triangular FE shape functions $N_i(x,y)$ yields the system of equations

$$K\underline{u} + \underline{g} = \underline{f} \tag{5}$$

with $\underline{u}$ containing the degrees of freedom for $\underline{A}_z$,

$$K_{ij} = \int_\Omega (\nu \nabla_{xy} N_i \cdot \nabla_{xy} N_j + \mathrm{j}\omega\sigma N_i N_j) \ \mathrm{d}\Omega \ , \tag{6}$$

$$\underline{f}_i = \int_\Omega \frac{\sigma}{\ell_z} \Delta \underline{V} \, N_i \, \mathrm{d}\Omega \ , \tag{7}$$

$$\underline{g}_i = -\int_{\partial\Omega} \nu \frac{\partial \underline{A}_z}{\partial n} \, N_i \, \mathrm{d}\Gamma \tag{8}$$

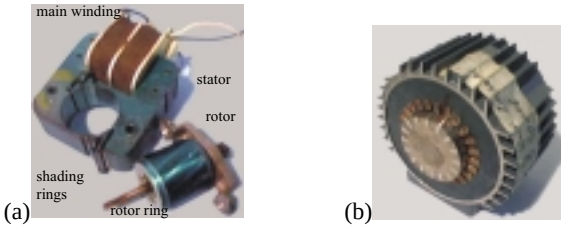

Fig. 2. (a) Shaded-pole motor and (b) capacitor motor.

and $\partial/\partial n$ the normal derivative outward to Ω. The terms $\underline{g}_i$ depend on the boundary conditions and vanish in case of the homogeneous Dirichlet or Neumann boundary conditions.

3. Slip transformation

Time-harmonic simulations are remarkably accurate and extremely efficient for the steady-state simulation of devices supplied with alternating currents. Unfortunately, accounting for motional effects in such simulations is not straightforward. Only in a very particular case, i.e., if the air gap field is a rotating wave, it is possible to account for motional eddy currents while keeping the classical time-harmonic formulation (4). Suppose the field at a circular interface between stator and rotor equals the rotating wave

$$A_z(\theta,t) = \mathrm{Re}\left\{\underline{c}_\lambda e^{\mathrm{j}(\omega t-\lambda\theta)}\right\} \tag{9}$$

with the phasor $\underline{c}_\lambda$, the wave number λ and the azimuthal coordinate θ along the interface (Fig. 1). An observer attached to the stator experiences the wave as a cosine rotating at the velocity ω/λ along the interface. A second observer is attached to the rotor and inherits the rotation at a constant mechanical velocity ω_m. The corresponding azimuthal coordinate θ' is related to θ by

$$\theta' = \theta - \omega_m t\ . \tag{10}$$

The second observer experiences the field at the interface as

$$A_z(\theta',t) = \mathrm{Re}\left\{\underline{c}_\lambda e^{\mathrm{j}\left((\omega-\lambda\omega_m)t-\lambda\theta'\right)}\right\} \tag{11}$$

which is also a rotating wave with the same phasor and pole pair number, but at a different pulsation $\omega_{s,\lambda} = \omega - \lambda\omega_m$, called the *slip pulsation*. Hence, phenomena at the stator side induce phenomena at the rotor side at slip pulsation. Motional eddy currents are easily incorporated in (4) by replacing the pulsation ω by the slip pulsation $\omega_{s,\lambda}$ for the rotating model parts. This procedure, called *slip transformation*, is equivalent to the scaling of the rotor impedances by the slip $s_\lambda = \omega_{s,\lambda}/\omega$ as is commonly done in equivalent circuit machine models. The assumption of a rotating wave form as field distribution in the air gap is approximately true for three-phase induction machines. Then, time-harmonic steady-state simulation with slip transformation commonly gives reliable results [1]. Slip transformation is however no longer applicable in the presence of non-negligible higher harmonic air gap fields, as for e.g. shaded-pole motors and capacitor motors (Fig. 2).

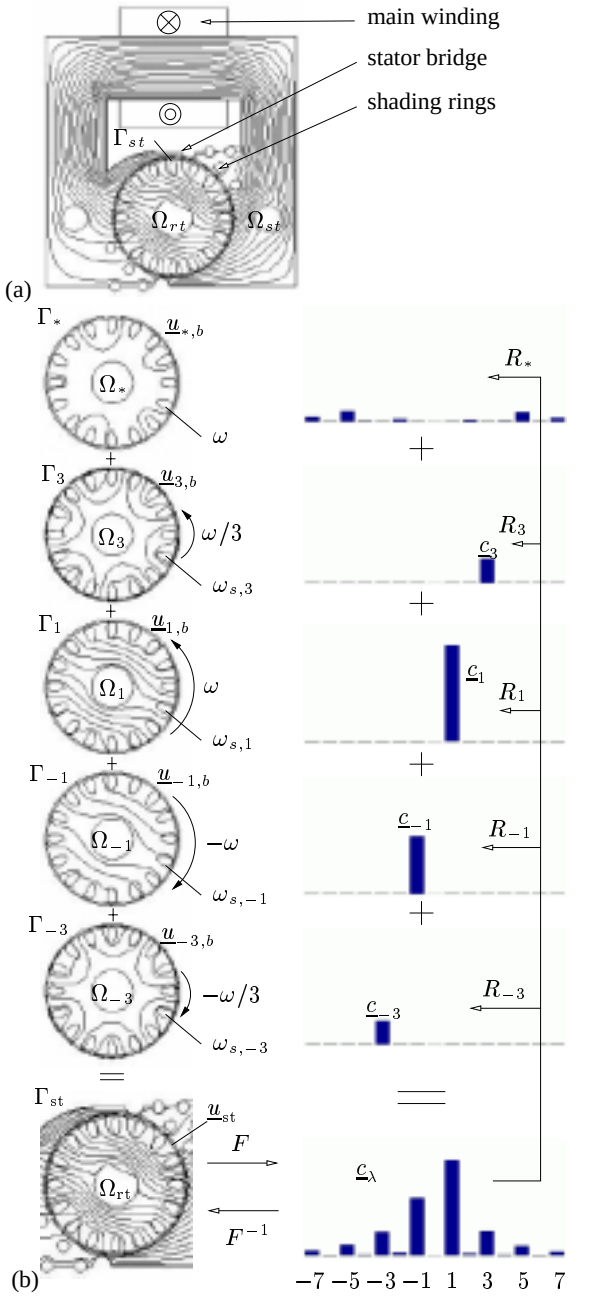

Fig. 3. Shaded-pole induction machine: (a) true solution and (b) spectral decomposition of the rotor flux: magnetic flux lines (left) and air gap magnetic flux density (right).

4. Air Gap Field Decomposition

Consider as an example the shaded-pole IM of Fig. 3a. The alternating field generated by the main winding is accomplished by a phase-lagging field originating from a few short-circuit rings distributed along the air gap [13]. The resulting elliptical air gap field consists of a large forward rotating and a smaller backward rotating component. Also the third harmonic components will introduce motional eddy currents which generate relevant torques. The Fourier de-

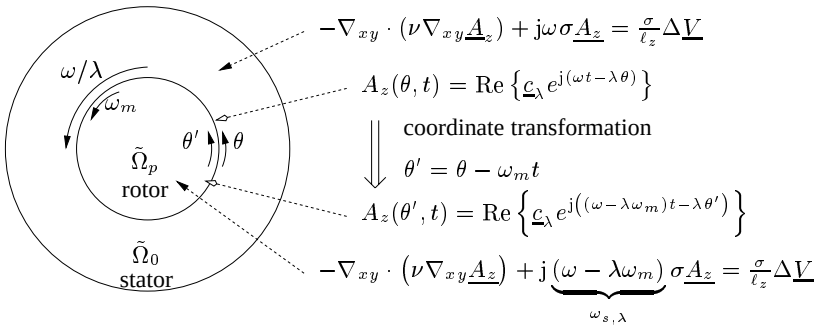

Fig. 1. Slip transformation technique, illustrated for a simplified machine model.

composition of the air gap field is

$$\underline{u}(\theta)=\sum_{\lambda=-\infty}^{+\infty}\underline{c}_\lambda e^{j(\omega t-\lambda\theta)} \tag{12}$$

where in this case $\underline{c}_1$, $\underline{c}_{-1}$, $\underline{c}_3$ and $\underline{c}_{-3}$ are particularly important. Using the common time-harmonic machine model and $\omega_{s,1}$ as the pulsation in the rotor region, all harmonic components are present in the rotor, but only the motional eddy current effects with respect to $\underline{c}_1$ are correctly taken into account. Obviously, the simulated currents and torques will be inaccurate.

The extension of the time-harmonic FE method, presented in this paper, allows the effects of higher harmonic air gap fields to be considered accurately without turning to transient simulation. The air gap field component with wave number λ will induce eddy current in the rotor at the slip pulsation

$$\omega_{s,\lambda}=\omega-\lambda\omega_m \tag{13}$$

which would be correctly taken into account if the pulsation applied at the rotor model part is defined by $\omega_{s,\lambda}$. To account for the true motional eddy current effects for all wave components individually, separate rotor models are required.

For the split-pole motor example, the relevant components of the air gap flux with coefficients $\underline{c}_\lambda$, $\lambda=\pm1,\pm3$, are distributed towards four distinct rotor models Ω_λ (Fig. 3b). Each rotor model experiences at its boundary Γ_λ a sinusoidal air gap wave rotating at the synchronous speed $\omega_{syn,\lambda}=\omega/\lambda$. As a consequence, the field in Ω_λ is time-harmonic with slip pulsation $\omega_{s,\lambda}=\omega-\lambda\omega_m$. To preserve the total flux, the remaining components with coefficients $\underline{c}_\lambda$, $\lambda\neq\pm1,\pm3$ are propagated to an additional rotor model Ω_*. They influence the saturation of the rotor teeth and generate inaccurate albeit small eddy currents in the rotor bars. The choice of the number of additional rotor models, the field components applied at their boundaries and the slip frequencies at which currents are induced, are based upon technical considerations motivated by the general rotating field theory for electrical machines. This choice can be adaptive, i.e., rotor models can be removed if their influence turns out to be negligible or added, e.g. if significant motional eddy current effects are observed at the rotor model hosting the set of remaining components.

5. Coupled finite element model

The air gap field decomposition is embedded in the FE model and resolved during the iterative solution of the FE system of equations. This strong coupled approach is necessary to maintain the effectiveness of the time-harmonic simulation scheme. Consider a model consisting of one stator model Ω_0 and n rotor domains Ω_p, $p=1,\ldots,n$ (see Fig. 4 for an example with $n=3$). The stator and rotor models share a circular interface Γ_b in the middle of the air gap. For each rotor domain, the slip pulsation $\omega_p=\omega-\lambda_p\omega_m$ is selected according to one of the field component applied at Ω_p, i.e., the component with pole pair number λ_p. A FE subsystem as in (5), is set up for each submodel Ω_p independently:

$$\begin{bmatrix} K_{p,aa} & K_{p,ab} \\ K_{p,ba} & K_{p,bb} \end{bmatrix}\begin{bmatrix} \underline{u}_{p,a} \\ \underline{u}_{p,b} \end{bmatrix}+\begin{bmatrix} 0 \\ \underline{g}_{p,b} \end{bmatrix}=\begin{bmatrix} \underline{f}_{p,a} \\ \underline{f}_{p,b} \end{bmatrix} \tag{14}$$

where the subscripts a and b distinguish between degrees of freedom associated with inner nodes of Ω_p and degrees of freedom associated with nodes at Γ_b. Since in general $\omega_{p_1}\neq\omega_{p_2}$, the FE stiffness matrices for the rotor domains are different although they feature the same FE mesh and reluctivities. The subsystems (14) are collected in a block system of equations:

$$\begin{bmatrix} K_{aa} & K_{ab} \\ K_{ba} & K_{bb} \end{bmatrix}\begin{bmatrix} \underline{u}_a \\ \underline{u}_b \end{bmatrix}+\begin{bmatrix} 0 \\ \underline{g}_b \end{bmatrix}=\begin{bmatrix} \underline{f}_a \\ \underline{f}_b \end{bmatrix}. \tag{15}$$

For convenience, assume all submodels have equidistant and matching grids at Γ_b.

An appropriate selection of rotating field components is performed by interface conditions applied at Γ_b:

$$F\underline{u}_{p,b}-R_pF\underline{u}_{0,b}=0,\quad p=1,\ldots,n \tag{16}$$

with F denoting the discrete Fourier transform and R_p a set of restriction operators such that $\sum_{p=1}^{n}R_p=I$. The choices of the sets $\{R_p\}$ and $\{\omega_p\}$ are motivated by the technical considerations described in the previous section. The effect of the interface conditions (16) is illustrated in Fig. 4. The interface conditions take the distribution of $\underline{A}_z$ at the stator side of Γ_b ($\underline{u}_{0,b}$), transform this into harmonic components ($F\underline{u}_{0,b}$), next restrict these to a particular subset ($R_pF\underline{u}_{0,b}$) and finally equal this subset of harmonics to the harmonic components of the distribution of $\underline{A}_z$ at one of the

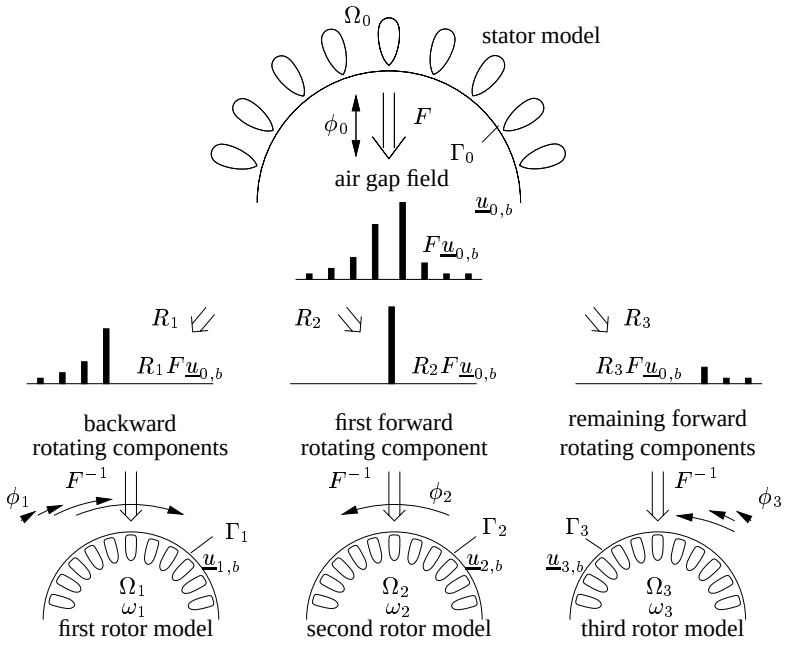

Fig. 4. Scheme of the air gap flux decomposition approach illustrating the splitting of the stator flux ϕ_0 into ϕ_1, ϕ_2 and ϕ_3.

rotor sides of Γ_b ($F\underline{u}_{p,b}$). The constraints (16) are collected in

$$B\underline{u}_b = 0 \tag{17}$$

with the constraint equation matrix

$$B = \begin{bmatrix} -R_1 F & F & & \\ \vdots & & \ddots & \\ -R_n F & & & F \end{bmatrix} . \tag{18}$$

The boundary integral terms $\underline{g}_{p,b}$ are resolved in terms of a set of Lagrange multipliers $\underline{\xi}$:

$$\underline{g}_b = B^H \underline{\xi} \, . \tag{19}$$

The Lagrange multipliers $\underline{\xi}$ are related to the Fourier coefficients of the magnetic field strengths along the rotor sides of the interface. The matrix factor B^H in (19) enforces an appropriate spectral decomposition of the magnetomotive force generated by the stator towards the different rotor models. The FE system (15) is combined with the constraint equations (17) and the boundary integral terms (19) resulting in the saddle-point problem

$$\begin{bmatrix} K_{aa} & K_{ab} & 0 \\ K_{ba} & K_{bb} & B^H \\ 0 & B & 0 \end{bmatrix} \begin{bmatrix} \underline{u}_a \\ \underline{u}_b \\ \underline{\xi} \end{bmatrix} = \begin{bmatrix} \underline{f}_a \\ \underline{f}_b \\ 0 \end{bmatrix} \tag{20}$$

The coupled system of equations (20) is solved by a specialised iterative solution technique described in detail in [14]. The matrix block B is never constructed in practice. Instead, the matrix-vector products and preconditioning steps invoked by the iterative solver apply Fast Fourier Transforms for F and F^{-1} and restriction operations for R_p. This approach with air gap field decomposition is easily generalised to boundary element models [15], to 3D FE models and to harmonic balance FE formulations [16, 17]. The restriction of equidistant and matching discretisations at the interface Γ_b can be loosened by applying non-equidistant Fourier transforms and mortar FE techniques [11] respectively. This is, however, disadvantageous for the efficiency of the simulation scheme since the Fast Fourier Transform algorithms can not longer be applied for F and F^{-1}. Solving (20) for the shaded-pole induction machine example immediately results in the flux in all rotor model parts Ω_p and the stator model part Ω_0 (Fig. 3).

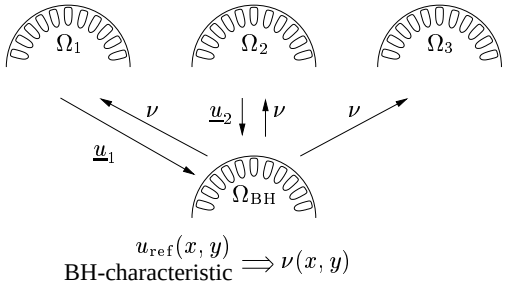

Fig. 5. Outer iteration accounting for ferromagnetic saturation at an additional rotor model Ω_{BH}.

6. Ferromagnetic saturation

The air gap flux decomposition approach is a spectral superposition technique. In order to incorporate non-linear effects such as ferromagnetic saturation, an outer non-linear iteration is set up. Between two linear steps, the true solution is reconstructed by combining the solutions of all rotor model parts at an additional rotor model Ω_{BH} (Fig. 5). In order to reduce the cost of determining the new set of reluctivities, only the partial solutions corresponding to a reduced set of rotor model $\mathcal{S}$, e.g. those with the largest amplitudes, are selected (only $\underline{u}_1$ and $\underline{u}_2$ in Fig. 5). After inverse Fourier transformation, the true solution for the rotor field at a num-

ber of time instants is obtained:

$$u_{\mathrm{ref}}(x,y) = \sum_{q\in\mathcal{S}} \underline{u}_q(x,y)e^{\mathrm{j}\omega_q t}\ . \tag{21}$$

For each time instant, a reluctivity pattern is evaluated applying the BH-characteristic of the ferromagnetic material. The reluctivity pattern is averaged in time and copied to all rotor models and defines the linearisation point for the next step of the outer iteration. This procedure neglects the variation in time of the reluctivity. This can be incorporated in a multi-harmonic FE approach [16] but is technically irrelevant for the models considered here.

7. External circuit coupling

To obtain a reliable 2D FE machine model, the influence of additional impedances representing stator end-windings, rotor end-bars, rotor ring, external sources and loads has to be taken into account [12, 1]. If a moving rotor is submitted to an air gap field consisting of components with different harmonic orders, the currents in the rotor bars or windings will contain components at the corresponding slip frequencies. Similarly as for the FE rotor models, the circuit parts connected to the rotor have to be considered for each harmonic component of currents and voltages separately. Inductances and capacitances present in the rotor circuits have to be adjusted according to the slip frequency. Especially, the skin effect in the rotor ring causes component at higher slip frequencies to experience a considerably higher resistance. The field-circuit coupling scheme used for the simulation of the technical models is described in detail in [18] and results in a few circuit equations added to the system of equations (20).

8. Shaded-pole induction machine

The magnetic flux lines computed for the shaded-pole induction machine example clearly reflect the wave numbers of the individual rotor fields (Fig. 3). The major components in Ω_* are the fifth harmonics. From the magnitude of the solution in Ω_*, one can decide to insert additional rotor models, e.g., to consider motional eddy currents with respect to $\underline{c}_5$ and $\underline{c}_{-5}$. The external circuit contains a voltage source exciting the main winding, impedances modelling the end-windings, end-bars and rotor ring and short-circuit connections for the shading rings. Significant saturation is observed at the stator bridges.

9. Capacitor motor

The air gap flux decomposition technique is applied to a capacitor motor (Fig. 2b). The main winding is fed by a 50 Hz alternating current supply and generates an alternating flux in the air gap. This flux is augmented by a flux generated by an auxiliary winding which is put in the quadrature axis with respect to the main winding and is connected to the same supply through a capacitor. As the additional flux is detuned both in space and time, the total air gap field is elliptical. The fundamental forward and backward rotating

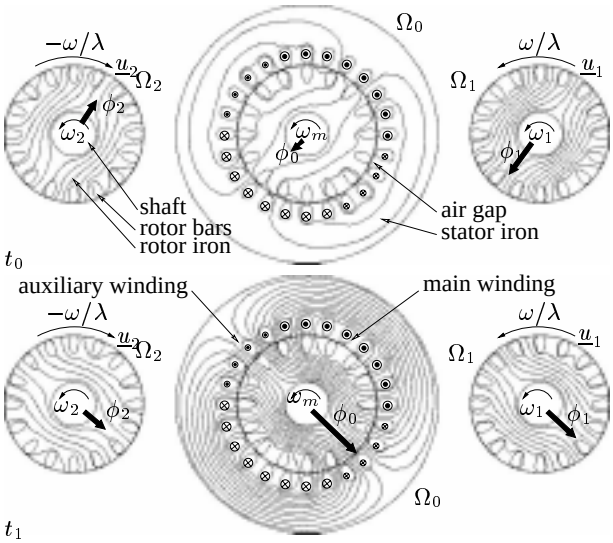

Fig. 6. Plot of the magnetic flux lines at t_0 and t_1 of a capacitor motor operating at 1500 rotations per minute.

air gap flux components, i.e., those with pole pair numbers 1 and -1, produce the most important torque components. The air gap field components with pole pair numbers 3 and -3 also induce significant eddy current effects. Especially for velocities close to the corresponding synchronous speeds 1000 rpm and -1000 rpm, these effects will influence the generated torque. The use of an external circuit coupling is indispensable to model the voltage excitation, the phase shift between main winding and auxiliary winding applied by the capacitor and the additional impedances modelling the end parts and connections of the stator windings and the rotor squirrel cage outside the 2D FE model. Four rotor models are considered: Ω_1 for the forward rotating field with pole pair number 1, Ω_2 for the backward rotating field with pole pair number -1, Ω_3 for the forward rotating field with pole pair number 3 and Ω_4 for all remaining air gap field components. The applied slip pulsations are $\omega_1 = \omega - \omega_m$ at Ω_1, $\omega_2 = \omega + \omega_m$ at Ω_2, $\omega_3 = \omega - 3\omega_m$ at Ω_3 and $\omega_4 = \omega + 3\omega_m$ at Ω_4. Hence, only motional eddy current effects with respect to the rotating air gap field components with orders ±1 and ±3 are correctly taken into account. In analogy to three-phase induction machines, this simplication is acceptable. If the rotor model Ω_4 hosting the remaining air gap harmonics would reflect a significant e.g. 5th order component, one can decide to add additional rotor models. In Fig. 6, the magnetic flux is plotted for the fundamental forward and backward rotating components at two instants of time t_0 and t_1 where t_1 is a quarter of a period shifted in time from t_0. The flux patterns show the alternating true rotor field ϕ_0 and the rotating rotor fields ϕ_1 and ϕ_2. The spectrum of the air gap flux indicates the importance of the higher harmonic air gap fields (Fig. 7). The capacitor motor model is used to compute the stationary speed-torque characteristic (Fig. 8). The characteristic clearly illustrates the effect of the third harmonic air gap field around 1000 rpm. This phenomenon is not correctly taken into account by classical time-harmonic FE models. Transient simulation incorporates the phenomenon but is substantially more expensive than the simulation scheme proposed here.

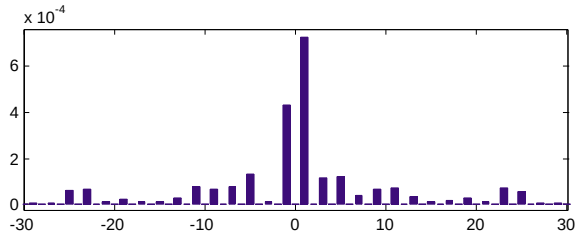

Fig. 7. Spectrum of the field in the air gap of the capacitor motor.

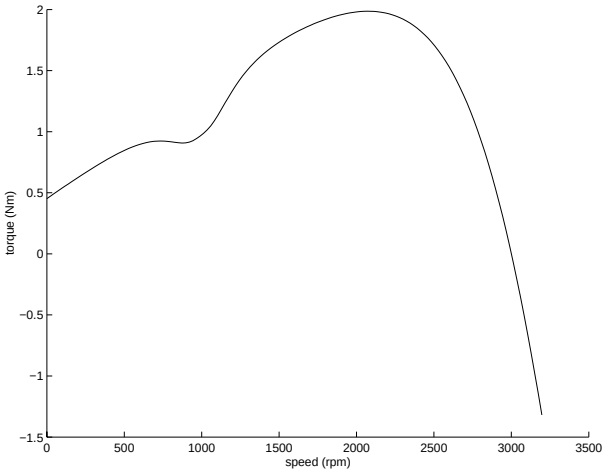

Fig. 8. Stationary speed-torque characteristic of the capacitor motor indicating a torque dip around 1000 rpm.

10. Conclusions

Inexpensive time-harmonic finite element simulation of electrical machines incorporating higher harmonic air gap field effects is made possible by spectrally decomposing the air gap field and distributing the higher harmonics to different rotor models. The models accounts for ferromagnetic saturation and external circuit coupling. The simulations of a shaded-pole induction machine and a capacitor motor reveal the influence of the backward first harmonic and the higher harmonic air gap fields and illustrate the convenience of the approach for simulating steady-state operating conditions of rotating electrical machines.

Acknowledgement

H. De Gersem is working in the cooperation project “DA-WE1 (TEMF/GSI)” with the “Gesellschaft für Schwerionenforschung (GSI)”, Darmstadt. The authors would like to thank ATB Austria for providing the material data of the capacitor motor.

References

[1] R. De Weerdt, E. Tuinman, K. Hameyer, and R. Belmans, “Finite element analysis of steady state behavior of squirrel cage induction motors compared with measurements,” *IEEE Transactions on Magnetics*, vol. 33, no. 2, pp. 2093–2096, Mar. 1997.

[2] E. Vassent, G. Meunier, and J.C. Sabonnadière, “Simulation of induction machine operation using complex magnetodynamic finite elements,” *IEEE Transactions on Magnetics*, vol. 25, no. 4, pp. 3064–3066, July 1989.

[3] G. Vinsard and B. Laporte, “A new formulation for induction machine computation,” *IEEE Transactions on Magnetics*, vol. 30, no. 5, pp. 3693–3696, Sept. 1994.

[4] H. De Gersem and K. Hameyer, “Air gap flux splitting for the time-harmonic finite element simulation of single-phase induction machines,” *IEEE Transactions on Magnetics*, vol. 38, no. 2, pp. 1221–1224, Mar. 2002.

[5] A. Arkkio, “Finite element analysis of cage induction motors fed by static frequency converters,” *IEEE Transactions on Magnetics*, vol. 26, no. 2, pp. 551–554, Mar. 1990.

[6] N. Sadowski, R. Carlson, S.R. Arruda, C.A. da Silva, and M. Lajoie-Mazenc, “Simulation of single-phase induction motor by a general method coupling field and circuit equations,” *IEEE Transactions on Magnetics*, vol. 31, no. 3, pp. 1908–1911, May 1995.

[7] A. Demenko, “Movement simulation in finite element analysis of electric machine dynamics,” *IEEE Transactions on Magnetics*, vol. 32, no. 3, pp. 1553–1556, May 1996.

[8] S. Kurz, J. Fetzer, G. Lehner, and W.M. Rucker, “A novel formulation for 3D eddy current problems with moving bodies using a Lagragian description and FEM-BEM coupling,” *IEEE Transactions on Magnetics*, vol. 34, no. 5, pp. 3068–3073, Sept. 1998.

[9] P. Alotto, A. Bertoni, I. Perugia, and D. Schötzau, “Discontinuous finite element methods for the simulation of rotating electrical machines,” *COMPEL*, vol. 20, no. 2, pp. 448–462, 2001.

[10] D. Rodger, H.C. Lai, and P.J. Leonard, “Coupled elements for problems involving movement,” *IEEE Transactions on Magnetics*, vol. 26, no. 2, pp. 548–550, Mar. 1990.

[11] A. Buffa, Y. Maday, and F. Rapetti, “Calculation of eddy currents in moving structures by a sliding mesh-finite element method,” *IEEE Transactions on Magnetics*, vol. 36, no. 4, pp. 1356–1359, July 2000.

[12] I.A. Tsukerman, A. Konrad, G. Meunier, and J.C. Sabonnadière, “Coupled field-circuit problems: trends and accomplishments,” *IEEE Transactions on Magnetics*, vol. 29, no. 2, pp. 1701–1704, Mar. 1993.

[13] V. József and B. Djura, “Analysis of the characteristics of single phase shaded pole induction motor with two short-circuited auxiliary phases,” *IEEE Transactions on Energy Conversion*, vol. 12, no. 4, pp. 269–274, Dec. 1997.

[14] H. De Gersem, M. Clemens, and T. Weiland, “Interface preconditioners for non-trivial interface conditions in air gaps of rotating electrical machines,” in *14th International Conference on Domain Decomposition Methods (DD14)*, Cocoyoc, Morelos, Mexico, Jan. 2002, pp. 68–69.

[15] K. Davey, “Rotating field analysis using boundary element method,” *IEEE Transactions on Magnetics*, vol. 35, no. 3, pp. 1402–1405, May 1999.

[16] S. Yamada, K. Bessho, and J. Lu, “Harmonic balance finite element method applied to nonlinear AC magnetic analysis,” *IEEE Transactions on Magnetics*, vol. 25, no. 4, pp. 2971–2973, July 1989.

[17] J. Gyselinck, P. Dular, C. Geuzaine, and W. Legros, “Harmonic-balance finite-element modeling of electromagnetic devices: a novel approach,” *IEEE Transactions on Magnetics*, vol. 38, no. 2, pp. 521–524, Mar. 2002.

[18] H. De Gersem, R. Mertens, U. Pahner, R. Belmans, and K. Hameyer, “A topological method used for field-circuit coupling,” *IEEE Transactions on Magnetics*, vol. 34, no. 5, pp. 3190–3193, Sept. 1998.